Biomedicine & Pharmacotherapy 167 (2023) 115469

Contents lists available at ScienceDirect

Biomedicine & Pharmacotherapy

journal homepage: www.elsevier.com/locate/biopha

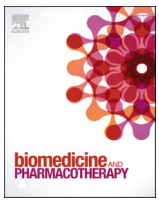

Lysyl oxidase-dependent extracellular matrix crosslinking modulates calcification in atherosclerosis and aortic valve disease

Carme Ballester-Servera [a,b,c], Judith Alonso [a,b,c], Laia Cañes [a,b,c], Paula Vázquez-Sufuentes [a,c], Lídia Puertas-Umbert [b,c,d], Amaya Fernández-Celis [e], Manel Taurón [b,c,f], Antonio Rodríguez-Sinovas [b,g], Natalia López-Andrés [e], Cristina Rodríguez [b,c,d,*,1], José Martínez-González [a,b,c,**,1]

[a] Instituto de Investigaciones Biomédicas de Barcelona-Consejo Superior de Investigaciones Científicas (IIBB-CSIC), Barcelona, Spain
[b] CIBER de Enfermedades Cardiovasculares, Instituto de Salud Carlos III, Madrid, Spain
[c] Institut d'Investigació Biomèdica Sant Pau (IIB SANT PAU), Barcelona, Spain
[d] Institut de Recerca Hospital de la Santa Creu i Sant Pau (IRHSCSP), Barcelona, Spain
[e] Cardiovascular Translational Research, Navarrabiomed, IdiSNA, UPNA, Hospital Universitario de Navarra (HUN), Pamplona, Spain
[f] Departamento de Cirugía Cardíaca, Hospital de la Santa Creu i Sant Pau-Universitat Autònoma de Barcelona (HSCSP-UAB), Barcelona, Spain
[g] Cardiovascular Diseases Research Group, Vall d'Hebron University Hospital and Research Institute, Barcelona, Spain

ARTICLE INFO

Keywords:
Lysyl oxidase
Cardiovascular calcification
Atherosclerosis
Extracellular matrix remodeling

ABSTRACT

Extracellular matrix (ECM) is an active player in cardiovascular calcification (CVC), a major public health issue with an unmet need for effective therapies. Lysyl oxidase (LOX) conditions ECM biomechanical properties; thus, we hypothesized that LOX might impact on mineral deposition in calcific aortic valve disease (CAVD) and atherosclerosis. LOX was upregulated in calcified valves from two cohorts of CAVD patients. Strong LOX immunostaining was detected surrounding calcified foci in calcified human valves and atherosclerotic lesions colocalizing with RUNX2 on valvular interstitial cells (VICs) or vascular smooth muscle cells (VSMCs). Both LOX secretion and organized collagen deposition were enhanced in calcifying VICs exposed to osteogenic media. β-aminopropionitrile (BAPN), an inhibitor of LOX, attenuated collagen deposition and calcification. VICs seeded onto decellularized matrices from BAPN-treated VICs calcified less than cells cultured onto control scaffolds; instead, VICs exposed to conditioned media from cells over-expressing LOX or cultured onto LOX-crosslinked matrices calcified more. Atherosclerosis was induced in WT and transgenic mice that overexpress LOX in VSMC ($TgLOX^{VSMC}$) by AAV-PCSK9D374Y injection and high-fat feeding. In atherosclerosis-challenged $TgLOX^{VSMC}$ mice both atherosclerosis burden and calcification assessed by near-infrared fluorescence (NIRF) imaging were higher than in WT mice. These animals also exhibited larger calcified areas in atherosclerotic lesions from aortic arches and brachiocephalic arteries. Moreover, LOX transgenesis exacerbated plaque inflammation, and increased VSMC cellularity, the rate of RUNX2-positive cells and both connective tissue content and collagen cross-linking. Our findings highlight the relevance of LOX in CVC and postulate this enzyme as a potential therapeutic target for CVC.

Abbreviations: AAV,, adeno-associated virus vector; BAPN,, β-aminopropionitrile; CAVD,, calcific aortic valve disease; CVC,, cardiovascular calcification; DHE,, dihydroethidium; DKK-1,, Dickkopf-related protein 1; ECM,, extracellular matrix; HC,, High cholesterol; HF,, High fat; LDLR,, low-density lipoprotein receptor; LOX,, Lysyl oxidase; LOXL,, LOX-Like; NIRF,, Near-Infrared Fluorescence; OM,, osteogenic media; OPG,, osteoprogeterin; OPN,, Osteopontin; ORO,, Oil Red O; RUNX2,, Runt-related transcription factor 2; α-SMA,, α-smooth muscle actin; TNAP,, Tissue non-specific alkaline phosphatase; VICs,, valvular interstitial cells; VSMCs,, vascular smooth muscle cells; WT,, wild-type.

* Correspondence to: IRHSCSP, C/Antoni Mª Claret, 08025 Barcelona, Spain.
** Correspondence to: IIBB, Rosselló, 161, 08036 Barcelona, Spain.
E-mail addresses: crodriguezs@santpau.cat (C. Rodríguez), jose.martinez@iibb.csic.es (J. Martínez-González).
[1] These authors contributed equally to this work.

https://doi.org/10.1016/j.biopha.2023.115469
Received 13 July 2023; Received in revised form 30 August 2023; Accepted 7 September 2023
Available online 18 September 2023

1. Introduction

Cardiovascular calcification (CVC) is a major health problem worldwide and an independent predictor of adverse cardiovascular events and all-cause mortality. In vascular calcification (VC) and calcific valve disease (CAVD), the most common forms of this disorder, calcium deposits are formed in the vessel wall and in the heart valve leaflets. Ectopic CVC results in tissue damage and organ dysfunction. Microcalcifications in atherosclerotic lesions of the intima have been related to detrimental effects on vascular compliance and vasomotion and to a higher risk of fibrous cap rupture [1,2]. In fact, coronary calcification is clinically considered as a negative prognostic factor and a marker for disease progression [3,4]. Likewise, CAVD is the most common cardiac valve disease and the main trigger of aortic stenosis. Indeed, CAVD is a highly prevalent disease which affects up to 10 % of adults older than 65 years and results in compromised valve function, cardiac pressure overload and eventually heart failure [5,6]. Unraveling the mechanisms underlying CVC is critical for the development of effective therapeutic and diagnostic tools. Although significant advances have been made in understanding the pathophysiology of these diseases, currently, there are no proven pharmacological tools to halt or slow down the course of CVC, hampering the management of these patients, for whom, surgery or transcatheter valve replacement are the only therapeutic options.

Nowadays, CVC is recognized as a complex and active process that resembles bone ossification [7–9]. This is a finely tuned disorder that encompasses the loss of anticalcific mechanisms, dysregulated mineral metabolism, osteoblastic cell transdifferentiation, inflammation, cell death and the release of calcifying extracellular vesicles, among others [7–10].

CVC requires the activation of signaling pathways and the upregulation of key genes/proteins involved in the osteogenic reprogramming and calcification of valve interstitial cells (VICs) and vascular smooth muscle cells (VSMCs), among them, RUNX2, a transcription factor essential for osteogenic transdifferentiation and mineralization [11,12]. The mechanisms underlying CVC are still not fully understood, but are actively investigated [7,13]. Notably, extracellular matrix (ECM) remodeling has emerged as a critical player in biomineralization, with collagen fibrils acting as the main scaffolding that favors mineral deposition and guides the growth of hydroxyapatite crystals [14–17]. Moreover, several studies suggest that collagen post-translational modifications, in particular collagen crosslinking, might play an integral role in ectopic matrix mineralization [18,19].

Lysyl oxidase (LOX) is the archetypal member of a family of copper-dependent enzymes (LOXs) that catalyzes the oxidative deamination of lysyl and hydroxylysyl residues in collagen chains, the first step in the formation of inter- and intra-catenary covalent cross-linkages, responsible for the mechanical properties of connective tissues. LOX dysregulation underlies the development of multiple cardiovascular diseases [20–23]. In the last years, we and others have shown that LOX preserves endothelial homeostasis [24–27], and modulates VSMC proliferation and neointimal thickening [28,29], but also contributes to vascular oxidative stress and arterial stiffness [30–32], as well as cardiovascular remodeling and fibrosis [33,34]. Recently, we reported that VSMCs calcification involves increased deposition of highly crosslinked collagen, and demonstrated the impact of LOX on this process [18]. Indeed, using complementary gain- and loss-of-function approaches we highlighted the potential contribution of LOX to VSMC mineralization and osteoblastic commitment *in vitro* [18]. However, the pathophysiological relevance of LOX to VC *in vivo* is essentially unknown and its role in CAVD virtually unexplored. To investigate this, analysis in human calcified aortic valve leaflets and human atherosclerotic plaques, gain-and loss-of-function studies in VICs and *in vivo* approaches in a genetically modified mouse model that specifically overexpresses LOX in VSMCs were carried out. Our results provide evidence about the active contribution of LOX to CVC, support the importance of ECM remodeling in this disorder, and suggest that targeting ECM or ECM-modifying enzymes could become potential therapeutic approaches to limit CVC.

2. Material and methods

2.1. Human samples

Two cohorts of CAVD patients referred for aortic valve replacement to the Hospital de la Santa Creu i Sant Pau (HSCSP; Barcelona, Spain) or to the Hospital Universitario de Navarra (HUN) were included in the study. According to their macroscopic degree of calcification, valve samples collected in the HSCSP were classified into two categories: those in which less than 20 % of the sample was calcified (low-calcified) and valves in which calcification involves more than 80 % of the specimen (high-calcified). These valves were rapidly stored at − 80 °C for posterior RNA/protein extraction or processed for immunohistochemical analysis. Some valves were dissected for the isolation of VICs (see below). Calcified valves from the HUN were used to analyze the expression of LOXs isoforms taking healthy autopsy specimens as a reference group. In this case, a part of calcified valves was visually dissected in areas with weak, mild, or severe calcification and separately processed for RNA extraction. This study was approved by the respective Institutional Research Ethics Committees (HSCSP's Research Ethics Committee; approval number: 19/267 and Comité Ético de Experimentación Clínica, Gobierno de Navarra, Departamento de Salud; number: 17/2013).

Human coronary artery samples were collected from patients undergoing heart transplant at the HSCSP prior approval by the HSCSP's Ethics Committee (approval number: 19/267). Human femoral arteries were collected from patients undergoing cardiovascular surgery at the Hospital Clínico Universitario Virgen de la Arrixaca (Murcia, Spain) in accordance to the Research Ethics Committee (approval number: 02/10). All studies involving human samples were performed in accordance with the Declaration of Helsinki of 1975, revised in 2013, and a written informed consent was obtained from all patients or legal representatives.

2.2. Isolation and culture of VICs

Once collected, valve leaflets were extensively washed in PBS and minced in small pieces under a sterile hood. The tissue was digested using 1 mg/mL collagenase type 2 (LS004176, Worthington Biochemical, Lakewood, NJ, USA) in PBS for 1 h at 37 °C under shaking, as described [35]. After digestion, the tissue was centrifuged for 5 min at 500 x *g* and the resulting pellet resuspended in DMEM/ F-12 supplemented with 20 % fetal bovine serum (FBS; Thermo Fisher Scientific, Waltham, MA, USA), 50 ng/mL insulin and 10 ng/mL fibroblast growth factor 2 (FGF2) and antibiotics. Isolated cells were platted on gelatin-coated flasks and subcultured. VICs were characterized by immunofluorescence showing positive staining for α-smooth muscle actin (α-SMA) and vimentin and negative for CD31, as described [35]. Mycoplasma contamination was excluded using the Venor®GeM qOneStep kit (Minerva Biolabs,GmbH; Berlin, Germany). Calcification was induced in low-passage VICs (passages 3–4) by exposure to an osteogenic media (OM; high glucose DMEM supplemented with 5 % FBS, 2 mmol/L Na_2HPO_4 and 50 μg/mL L-ascorbic acid). The impact of the pharmacological inhibition of LOX on VICs calcification was assessed by incubation with β-aminopropionitrile (BAPN; CAS 2079–89–2; 500 μM added 24 h before osteogenic induction, refreshing the medium every 3 days), a specific inhibitor of LOX activity. Further, in some experiments, VICs cultured under osteogenic conditions were treated for 4 d with conditioned media from confluent VICs transduced with the pLVX/LOX lentiviral expression vector or the corresponding empty vector [28]. In this approach, the conditioned medium accounts for 33 % of the final volume of OM.

2.3. Calcium assessment in cell culture

Alizarin Red staining was used to visualize calcium deposition in cell culture, as described [18]. Tissue non-specific alkaline phosphatase (TNAP) activity was measured in cell lysates using the Alkaline Phosphatase Activity Colorimetric Assay Kit (Ref K412; BioVision, Abcam, Waltham, MA, USA).

2.4. Real-time PCR

Total RNA was purified using the TriPure Isolation Reagent (Roche Diagnostics, Mannheim, GE) according to manufacturer's instructions. RNA was reverse transcribed into cDNA using the High Capacity cDNA Reverse Transcription Kit (Applied Biosystems, Foster City, CA, USA) and the quantification of mRNA levels was performed by real-time PCR using an ABI PRISM 7900HT sequence detection system (Applied Biosystems) and specific primers and probes (provided by the Assay-on-Demand system; Applied Biosystems or Integrated DNA Technologies, Coralville, IA, USA) as follows: *LOX* (Hs_00942480_m1), LOX-like 1 (*LOXL1)* (Hs_00173746_m1), *LOXL2* (Hs_00158757_m1), *LOXL3* (Hs_00261671_m1), *LOXL4* (Hs_00260059) and Osteopontin (*OPN)* (Hs.PT.58.19252426). mRNA levels were also quantified by SYBR-Green real-time PCR analysis using specific oligonucleotides targeting human Runt-related transcription factor 2 (*RUNX2)* (5'- GTCATGGCGGGTAACGATGA-3' and 5'-AAACTCTTGCCTCGTCCACT-3') *GAPDH* was used as endogenous control (Hs.PT.39a.22214836). Relative mRNA levels were determined using the $2^{-\Delta\Delta Ct}$ method.

2.5. Western blotting

Whole-cell extracts were obtained from VICs monolayers using a lysis buffer containing 10 mM Tris-HCl (pH 7.4), 1 mM ortovanadate and 1 % SDS. Protein from human valves and mouse liver was extracted using a buffer containing 0.5 mM EGTA, 100 mM NaCl, 100 mM Glycerol-2-phosphate, 50 mM HEPES pH 7.4, 10 % Glycerol, 0.1 % Tween® 20 supplemented with 1X Protease Inhibitor Cocktail (Merck). To analyze secreted LOX protein levels in VICs' conditioned media, cells were exposed for 6 days to OM, serum starved for 48 h and cell supernatants were concentrated (20-fold) in PBS using Amicon™ Ultra-4 centrifugal filters (Merck Millipore, Burlington MA, USA). Protein lysates and cell-conditioned media were resolved under reducing conditions on dodecyl sulphate-polyacrilamide gel electrophoresis (SDS-PAGE) and electrotransferred onto Immobilon polyvinylidene difluoride membranes (IPVH00010, Immobilon, Merck-Millipore). Blots were blocked with 5 % non-fat dry milk and incubated overnight at 4 °C with specific antibodies against LOX (NB-100–2530, Novus Biologicals), OPN (NB-600–1043, Novus Biologicals), RUNX2 (ab23981, Abcam) and LDL receptor (LDLR) (3839–30, BioVision). Appropriate horseradish peroxidase-conjugated IgGs were used as secondary antibodies (Dako Products, Agilent). Membranes were developed using the Luminata™ Western HRP Substrate (Immobilon, Merck-Millipore). The molecular weight of detected proteins was estimated with a protein ladder (Hyperpage Prestained Protein Marker; Bioline, Paris, France or Protein Marker VI (10−245) prestained; PanReac, Applichem, Barcelona, Spain). ß-actin (A5441, Merck) was used as a loading control to verify equal loading in each lane. Original blots are shown in Supplementary Fig. S11.

2.6. LOX silencing and lentiviral overexpression of human LOX in VICs

LOX knockdown was carried out in VICs using small interfering RNAs (siRNAs) [18]. In brief, 25,000 cells/cm^2 were transfected into 12-well plates with a combination of 4 individual siRNAs supplied by the On-Target Plus SmartPool (Human LOX L-009810–00–0005; GE Healthcare Dharmacon, Lafayette, CO, USA). The ON-TARGET plus Non-targeting Control Pool (D-001810–10–05; GE Healthcare Dharmacon) was used as a control. siRNA delivery to VICs was accomplished using DharmaFECT1 Transfection Reagent (GE Healthcare Dharmacon). Specifically, cells were transfected with 30 nM siRNA, using 2 μl of DharmaFECT1 Transfection Reagent. After 8 h the medium was replaced, cells were allowed to recover overnight and then were exposed to the osteogenic media.

VICs were transduced with recombinant lentivirus to overexpress human LOX using the pLVX/LOX construct previously described [28]. The pLVX empty vector was used as control. Cells were transduced for 24 h with recombinant lentivirus. The transduced cell population was enriched by puromycin selection (5 days) before osteogenic induction.

2.7. Generation of decellularized VICs-derived ECM scaffolds

VICs transduced with the pLVX/LOX lentiviral construct (or the corresponding empty vector) or treated with or without BAPN were maintained under normal culture conditions for at least 5 days to allow cells to deposit a mature ECM. Then the culture medium was carefully aspirated, cell monolayers washed twice with PBS and cells detached with 0.05 % Triton X-100, 20 mM NH_4OH in PBS at 37 °C. Complete cell removal was monitored and confirmed under microscope. Then, the ECM scaffold was gently rinsed with PBS followed by two washes of PBS containing 1 mM $MgSO_4$ and 1 mM $CaCl_2$ to remove cellular debris. After a final wash with PBS, this procedure leaves the decellularized matrix intact, ready to VICs reseeding and osteogenic induction as described above.

2.8. Animal handling

In vivo approaches were performed in a transgenic mouse model that overexpresses human LOX specifically to SMC (TgLOX^{VSMC}) under a C57BL/6 J background [28,29,36]. Non-transgenic littermates were used as a control group (WT). Animals were housed in a pathogen-free area at the Animal Experimentation Unit (Institut de Recerca de l'Hospital de la Santa Creu i Sant Pau [IRHSCSP, Barcelona, Spain), under controlled temperature and humidity conditions (21 ± 1 °C), standard light-dark cycle (12 h light/dark) and fed regular chow *ad libitum*. TgLOX^{VSMC} mice were backcrossed with C57BL/6 J animals (Charles River Ltd; Kent, UK) and maintained under heterozygosis (39–42 generations). Procedures were approved by the IRHSCSP ethical committee (Law 5/June 21, 1995; Generalitat de Catalunya) and carried out according to the principles and guidelines required by the Spanish Policy for Animal Protection RD53/2013 and the European Union Directive 2010/63/UE.

Atherosclerosis and calcification were induced in 15-weeks-old male mice (both TgLOX^{VSMC} and WT) by a single tail vein injection to deliver a liver-tropic adeno-associated virus vector (AAV) encoding for the pathological human gain-of-function mutant of PCSK9 (AAV-PCSK9^{D374Y}) [37,38] (CNIC Viral Vectors Unit, Madrid, Spain), while saline was injected to control mice. Twenty-four hours later, mice were fed a HF (21 %) and HC (HF/HC) diet (1.25 %) (D12108C, Research Diets, New Brunswick, USA) for 20 weeks. Animals were randomly distributed in the different experimental groups using a computer random order generator. The order of measurements was also randomized and no animals were excluded from the study. At the end of the experimental period animals were anaesthetized (150 mg/Kg ketamine and 1 mg/Kg medetomidine; i.p.), euthanized by bilateral thoracotomy and the aorta and the first main branch of the aortic arch (the innominate artery) were dissected, cleaned and processed as follows: some aortas were fixed and used for en face Oil Red O (ORO) staining; innominate arteries and the entire aortic arches were fixed, and were embedded in paraffin or embedded in OCT (innominate arteries) and embedded in OCT (entire aortic arches) and sectioned for histological and immunohistochemical analysis; a second group of aortas were rapidly frozen in liquid N_2 and stored at − 80 °C for mRNA and protein isolation; finally, to characterize atherosclerotic lesions in aortic sinus,

in some animals the heart and approximately 2 mm of the proximal aorta were harvested and cut adjusting the sectioning angle, thus performing a transversal incision on the heart perpendicular to the ascending aorta. Samples were paraffin-embedded or embedded in OCT and snap frozen for subsequent analysis. These assessments were performed in a blinded manner.

2.9. Ultrasound imaging

The ascending aorta and the innominate artery were visualized by ultrasonography one week before the beginning of the study and at the end of the experimental period to estimate luminal stenosis and confirm the presence of atherosclerotic lesions. Anaesthetized mice (1.5–2 % isoflurane) were placed on a heating pad (37 °C) in a supine position. The anterior chest wall was shaved and the ascending aorta and the innominate artery were visualized in one plane in the right parasternal long-axis view using a Vevo 2100 ultrasound with a 30 MHz transducer (VisualSonics, Toronto, ON, Canada).

2.10. Plasma analysis

Heparinized blood from 4 h-fasting mice was collected through the facial vein (submandibular) at 0, 1, 5 and 13 weeks after AAV-PCSK9^{D374Y} transduction and by cardiac punction at the end of the experimental procedure. Plasma levels of total cholesterol (Wako Cholesterol E, Wako Pure Chemicals), triglycerides (with glycerol blanking; L-type Triglyceride M, Wako Pure Chemicals), circulating human PCSK9 (Human PCSK9 Quantikine ELISA Kit), Osteoprogeterin (OPG; Mouse Osteoprogeterin Quantikine ELISA Kit), Dickkopf-related protein (Dkk-1; Mouse Dkk-1 Quantikine ELISA Kit, R&D Systems, Biotechne, Minneapolis, USA), calcium (Quanti chrom Calcium Assay, Bioassay Systems, Hayward, CA, USA) and phosphate (Phosphate Colorimetric Assay Kit, BioVision) were determined.

2.11. Oil Red O (ORO) staining of en face aortas

Atherosclerotic plaque burden was examined by en-face ORO staining of whole aorta. Aortas were dissected from PCSK9^{D374Y}-transduced TgLOX^{VSMC} and WT mice fed with a HF/HC diet for 20 weeks. Samples were cleaned of perivascular fat, fixed in 4 % paraformaldehyde/0.1 M PBS (pH 7.4) for 24 h and incubated into 78 % methanol for 5 min (2X). Subsequently, whole aortas were stained with freshly prepared ORO solution (0.2 % w/v for 60 min). After rinsing in 78 % methanol, stained aortas were opened longitudinally and mounted onto a smooth surfaced black wax petri dish exposing the luminal side. Images of whole aortas were captured and lesion area was measured, by a blinded operator, as percentage of total luminal area using the Image J software.

2.12. Analysis of macroscopic calcification by Near-Infrared Fluorescence (NIRF) imaging

Aortic macroscopic calcification was analyzed *ex vivo* using a fluorescently-conjugated bisphosphonate probe with high affinity for hydroxyapatite (Osteosense 680 EX probe (PerkinElmer, Waltham, MA, USA). Osteosense 680 EX (2 nmol/100 μl saline solution) was administered *via* tail vein injection to TgLOX^{VSMC} and WT mice transduced with the PCSK9^{D374Y} AAV vector and subjected to a HF/HC for 20 weeks. Then the hearts and aortas were dissected, fixed with 4 % paraformaldehyde and imaged 24 h post tail vein injection to map the NIRF signal. Total radiance efficiency was captured in a blinded manner by an IVIS Spectrum *In Vivo* Imaging System (PerkinElmer) by setting the excitation wavelength at 675 nm and the emission wavelength at 720 nm.

2.13. Histology and immunohistochemistry

Human valves and atherosclerotic arteries and murine vascular samples (innominate arteries, aortic arches and aortic sinus) were fixed in 4 % paraformaldehyde and embedded in paraffin or frozen and OCT-embedded. Paraffin Section (4 μm) were deparaffinized, rehydrated in a series of graded ethanol and rinsed in distilled water. Antigen retrieval was performed with 10 mM citrate buffer pH 6 or 10 mM Tris/1 mM EDTA pH 9 in a water bath set to 95–99 °C during 20 min. Then slides were immersed in a 3 % solution of hydrogen peroxide in methanol (30 min) to block endogenous peroxidase activity. Afterwards sections were incubated in 10 % normal serum, endogenous avidin and biotin was blocked (Vector Laboratories, Burlingame, CA, USA) and specific antibodies targeting LOX (ab31238), α-SMA (ab5694, Abcam), CD68 (ab125212, Abcam), RUNX2 (ab23981, Abcam), OPN (NB-600–1043, Novus Biologicals, Littleton, CO, USA), and vimentin (ab92547, Abcam) were applied. After extensive washing, sections were exposed to an appropriate biotinylated secondary antibody (Vector Laboratories, Burlingame, CA, USA) during 1 h, and subsequently to Vectastain (ABC) avidin-biotin peroxidase complex (Vector Laboratories) for 30 min. Finally, slides were incubated with 3,3'-diaminobenzidine (DAB) and counterstained with hematoxylin prior to be dehydrated and mounted. Negative controls without primary antibodies were run to exclude unspecific binding.

Conventional histological analysis was performed by hematoxylin-eosin (H&E) and the modified Russell-Movat pentachrome (Movat's) (Electron Microscopy Sciences, Hatfield, PA) staining. Lesion area in the innominate arteries, aortic arches and aortic sinus was determined by a blinded operator on H&E-stained sections using Image J software. Deposited calcium was labeled with the Osteosense 680 EX fluorescent probe (200 nM) or visualized by Von Kossa staining (Silver plating kit acc. to von Kossa, Merck, Darmstadt, Germany). Collagen content and crosslinking was determined by visualizing Picrosirius Red staining (Merck) under polarized light. α-SMA staining of innominate arteries allowed quantifying fibrous cap thickness. Results were expressed as positive cells *per* area (for RUNX2 and CD68) or as the percentage of positive area *vs*. total area concerning crosslinked collagen (birefringence of collagen fibers after picrosirius red staining), Alcian Blue (Movat's staining), calcification (von Kossa and Osteosense 680 EX stainings) OPN, and α-SMA.

2.14. Immunocytochemistry

Collagen deposition was visualized in VICs plated on 35-mm diameter μ-dishes (Ibidi, Martinsried, Germany) and subjected to OM for 8 days. Cells were fixed in ice-cold 4 % paraformaldehyde and non-permeabilized VICs were blocked with 1 % BSA-PBS. Then, VICs were incubated with an antibody against collagen Iα1 (NB600–408, 1:150; Novus Biologicals, Cambridge, U.K.) for 18 h. After washing, dishes were exposed to a fluorescence–conjugated secondary antibody (Goat Anti-Rabbit Alexa Fluor 488; Thermo Fisher Scientific). Cells were counterstained with Hoechst 33342 trihydrochloride trihydrate (H3570, Invitrogen) and samples mounted with ProLong™ Antifade Reagent mounting medium (Invitrogen). The extent of collagen deposition was visualized and acquired with an immunofluorescence microscopy (Olympus BX51). Controls without the primary antibody were included.

2.15. Statistical analysis

Results are shown as mean ± standard error of the mean (SEM). Significant differences were established by t-Test, two-way ANOVA analysis with repeated measures, one-way or two-way ANOVA followed by Tukey's post-hoc tests. When normality of data failed the Shapiro-Wilk test, the Mann-Whitney U test was used. Incidence of risk factors in CAVD patients was assessed by Fischer's exact test. Data were analyzed with the GraphPad Prism version 8.0.2. Sample-size was

estimated on the basis of our previous experience using the calculator https://www.imim.cat/ofertadeserveis/software-public/granmo/, considering an alpha risk of 0.05 and a beta risk of 0.2 in a two-sided test. Differences were considered significant at $P < 0.05$.

3. Results

3.1. LOX is upregulated in calcified valves

The expression of LOX and LOXL isoenzymes was analyzed in valve leaflets from CAVD patients who underwent aortic valve replacement at Hospital Universitario de Navarra (HUN) (Supplementary Table S1). In this study, controls were non-calcified valves from autopsy (mean age 76 ± 10; 55 % males), whose characteristics were previously reported [39]. Among LOXs isoenzymes, LOX exhibited the highest expression level in control valves, and was significantly upregulated in calcified specimens reaching higher expression than any other isoform (Fig. 1). Furthermore, in calcified valves, LOX was the only isoenzyme whose expression levels were higher in the most calcified areas of the valves compared to less mineralized zones (Supplementary Fig. S1), thus suggesting the contribution of LOX to CAVD.

The upregulation of LOX in calcified valves was confirmed in a second cohort of CAVD patients. Supplementary Table S2 compiles the clinical and demographic characteristics of patients included in the Hospital de la Santa Creu i Sant Pau (HSCSP) cohort, who were distributed into two groups according to the extent of valve calcification. There were no significant differences regarding age, sex, concomitant diseases, smoking or pharmacological treatments between patients whose valves were classified as low- and high-calcified. Patients providing low-calcified valves exhibited significantly less severe stenosis coupled with better echocardiographic parameters than those individuals from whom highly calcified samples came. LOX mRNA levels were significantly higher in extensively calcified valves compared with those with a low calcification grade (Fig. 2A). This was associated with an enhanced expression of both, RUNX2, a master transcription factor in osteogenic lineage commitment and a driver of aortic stenosis [11,12], and OPN, a recognized osteogenic marker [40]. This expression profile was similar to that detected by western blot, with a significant increase of protein levels for LOX as well for RUNX and OPN (Fig. 2B). Accordingly, immunohistochemical analysis of high-calcified valves revealed a strong immunostaining for LOX nearby calcified foci, detected by von Kossa staining. Notably, analysis of consecutive sections showed that LOX colocalizes with RUNX2 and OPN in vimentin positive cells (Fig. 2C, Supplementary Fig. S2). Extensively calcified valves also exhibited high superoxide anion levels (Supplementary Fig. S3). By contrast, in low-calcified samples, LOX was barely detected and DHE staining evidence low ROS production (Fig. 2C, Supplementary Fig. S3). Altogether, these data confirmed the upregulation of LOX in calcified human valves and suggest a prominent role of this isoform in CAVD.

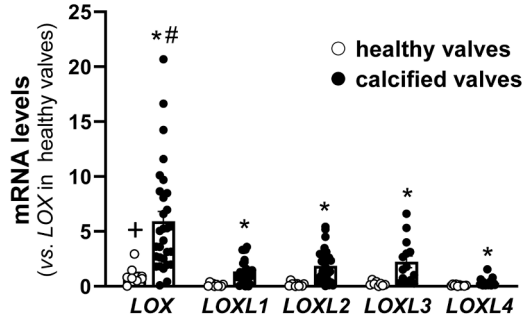

Fig. 1. Expression of LOX and LOXL isoenzymes in human calcific aortic valve disease (CAVD). The expression level of LOX and LOXL isoenzymes was assessed by real time PCR in valve leaflets from patients with CAVD recruited at Hospital Universitario de Navarra (n = 31; black symbols) or in healthy autopsy specimens (n = 16; white symbols). $P < 0.05$: *vs.* the same isoenzyme in healthy specimens; # *vs.* any of the other isoenzymes in calcified valves; + *vs.* any of the other isoenzymes in healthy specimens.

3.2. LOX is increased in calcifying VICs and exacerbates calcium deposition

Data described above prompted us to examine whether VICs calcification impacts on LOX expression. Human VICs cultured under osteogenic conditions showed an increased secretion of LOX in the growth media (Fig. 3A) and an enhanced deposition of organized collagen I (Fig. 3B), along with higher upregulation of osteogenic markers (Fig. 3A), exacerbated TNAP activity and stronger mineralization of the ECM than control cells (Fig. 3C).

To gain further insight into the role of LOX in CAVD, calcifying VICs were treated with BAPN in order to inhibit LOX activity. Interestingly, BAPN, that attenuated collagen I deposition (Fig. 4A), ameliorated matrix calcification in osteogenic media (OM)-induced cells (Fig. 4B). Effective LOX silencing similarly ameliorated matrix calcification in OM-induced cells (Supplementary Fig. S4). Moreover, because environmental cues importantly influence cell behavior, VICs were seeded onto decellularized ECM from either control or BAPN-treated cells and then exposed to osteogenic conditions. Cells growing on matrices from BAPN-treated cells were less mineralized than those cultured onto ECM produced by control VICs (Fig. 4C). Conversely, the effective lentiviral overexpression of LOX (Supplementary Fig. S5) exacerbated not only collagen deposition but also ECM mineralization (Fig. 5A-B). Further, the growth of VICs on crosslinked ECM from cells overexpressing LOX enhanced OM-induced matrix calcification compared with VICs plated onto matrices from control cells (pLVX-transduced) (Fig. 5C). Moreover, OM-induced VICs exposed to conditioned media from LOX-transduced cells exhibited a more pronounced calcification than those receiving cell supernatants from control cells (Fig. 5D). These results emphasize the role of extracellular and catalytically active LOX in ECM crosslinking that drives calcification of VICs.

3.3. LOX is highly expressed in calcified human atherosclerotic lesions and colocalizes with RUNX2

Our previous research in femoral and popliteal atherosclerotic lesions evidenced the existence of a significant correlation between LOX expression and arterial calcification [18]. Now, we have performed a more in-depth immunohistochemical analysis in consecutive sections from atherosclerotic femoral arteries, showing that the high expression of LOX detected in the vicinity of calcified regions corresponds to VSMC rich areas positive for RUNX2 (Fig. 6A). This profile is similar to that found in coronary artery calcifications from human advanced atherosclerotic lesions, in which LOX also colocalizes with immunoreactive RUNX2 in α-SMA-positive cells (Fig. 6B).

3.4. LOX overexpression in VSMC aggravates atherosclerosis and vascular calcification

Next, we aimed to better understand the contribution of LOX to atherosclerosis and vascular calcification by an *in vivo* approach. Transgenic mice that overexpress LOX in VSMC ($TgLOX^{VSMC}$) and their C57BL/6 J littermates (wild-type [WT]) were transduced with an adeno-associated virus vector (AAV) encoding for $PCSK9^{D374Y}$ and fed a HF/HC diet for 20 weeks to induce hypercholesterolemia, atherosclerosis and vascular calcification, as described [41], while control mice were injected with saline (Supplementary Fig. S6A). The HF/HC diet similarly increased body weight in all groups investigated (Supplementary Fig. S6B). As expected, AAV-$PCSK9^{D374Y}$ transduction led to an increase in circulating human PCSK9 levels (Supplementary Fig. S6C) and to a consequent drastic reduction of hepatic LDLR (Supplementary Fig. S6D) without differences between WT and $TgLOX^{VSMC}$ transduced mice, that

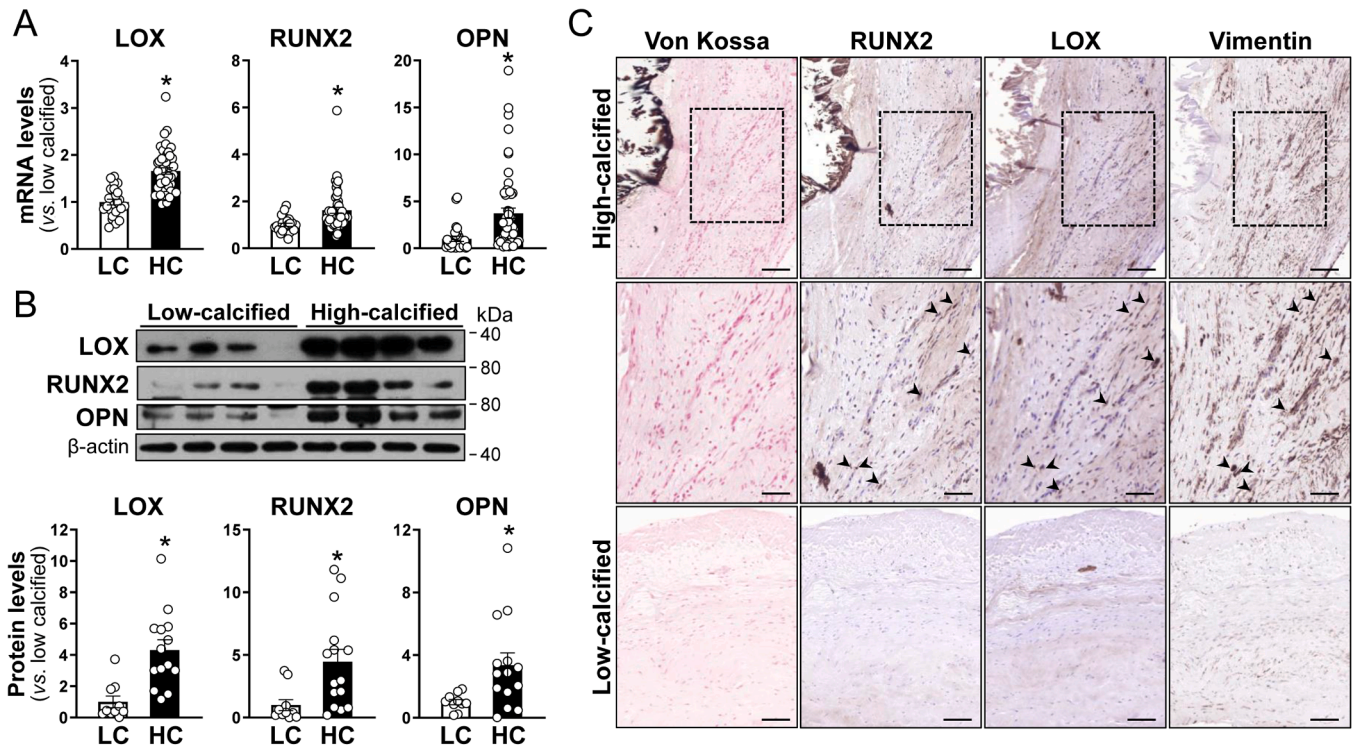

Fig. 2. LOX and osteogenic markers are upregulated in human calcific aortic valve disease. (A) mRNA levels of LOX, RUNX2 and osteopontin (OPN) in low- (LC; n = 26) and high-calcified (HC; n = 55) human aortic valves quantified by real-time PCR. Data are mean±SEM. * $P < 0.0001$ *vs*. LC. Significant differences were determined by Mann-Whitney test. (B) Representative immunoblot images showing LOX, RUNX2 and OPN protein levels in LC and HC human aortic valves, and bar graphs showing the result of the densitometric quantification of western blots. The levels of β-actin are shown as a loading control. Data are mean±SEM (n = 10–15). * $P < 0.05$ *vs*. LC. Significant differences were determined by Mann-Whitney test. (C) Representative images of Von Kossa staining and immunostainings for LOX, RUNX and vimentin in LC and HC human aortic valves. The indicated areas are magnified in central panels. Black arrowheads indicate positive cells for LOX, RUNX2 and vimentin detected in consecutive sections. Bars: 100 μm (upper and lower panels) and 50 μm (central panels).

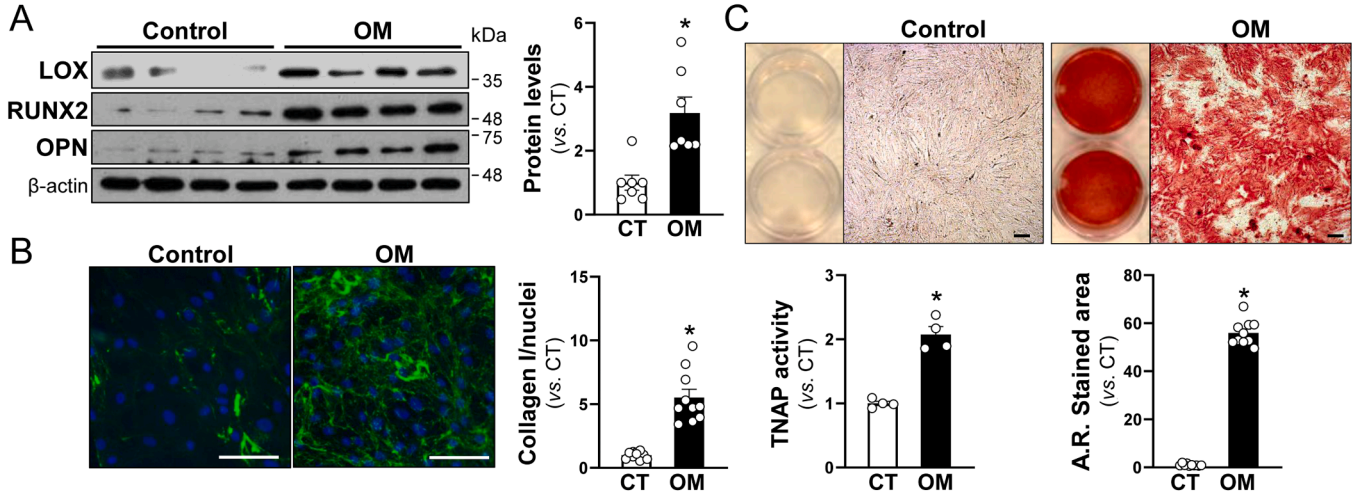

Fig. 3. LOX expression is enhanced in calcifying valvular interstitial cells (VICs). Human VICs were cultured in control media (CT, white bars) or in osteogenic media (OM, black bars). (A) Representative immunoblot images showing levels of secreted LOX, and RUNX2 and OPN levels expressed by these cells after osteogenic induction, and bar graphs showing the results of the densitometric quantification of western blots. The levels of β-actin are shown as a loading control. Data are mean ±SEM (n = 7). * $P < 0.01$ *vs.* control cells. Significant differences were determined by Mann-Whitney test. (B) Representative images showing type I collagen deposition in VICs cultured in CT and OM, and bar graphs showing the results of the immunofluorescence quantification (Bars: 200 μm). Data are mean±SEM (n = 10). * $P < 0.0001$ *vs.* control cells. Significant differences were determined by unpaired t test. (C) Representative images of Alizarin Red (AR) stainings from these cells after osteogenic induction (Bars: 100 μm), and bar graph showing both the results of the densitometric quantification of AR stainings (n = 10) and tissue-nonspecific alkaline phosphatase (TNAP) activity (n = 4). Data are mean±SEM. * $P < 0.05$ *vs.* CT. Significant differences were determined by Mann-Whitney test.

also exhibited a similar increase in total cholesterol and triglyceride plasma levels (Supplementary Fig. S6E-F).

The association of PCSK9^{D374Y} transduction with a long-lasting period of HF/HC diet in both WT and TgLOX^{VSMC} mice fostered the development of atheromatous lesions, that became manifest by ultrasound imaging at the brachiocephalic trunk, as an overt luminal stenosis

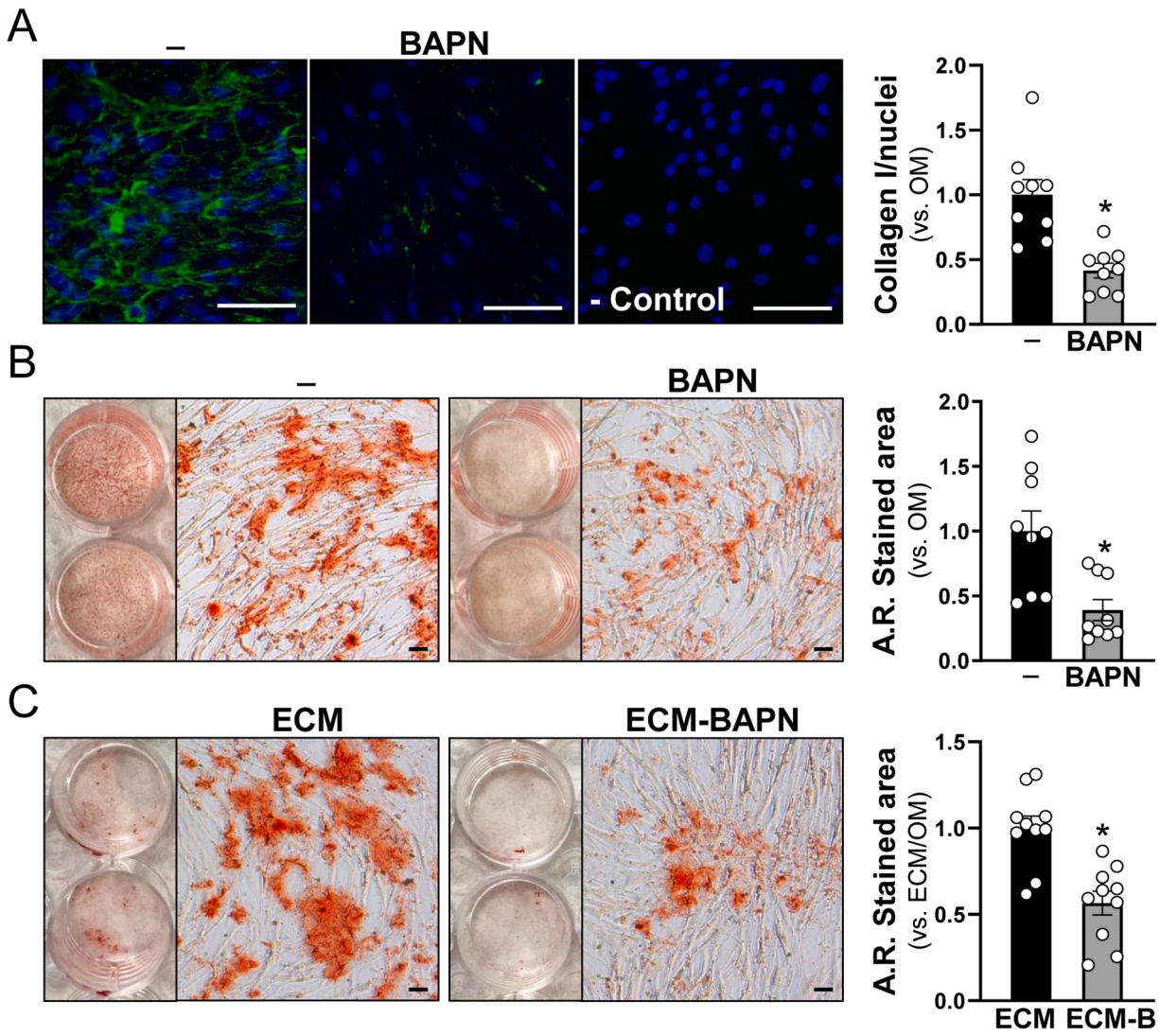

Fig. 4. Inhibition of LOX activity prevents valvular interstitial cells (VICs) calcification. (A-B) Human VICs were cultured under osteogenic conditions in the presence or absence of 0.5 mM BAPN (β-aminopropionitrile; inhibitor of LOX activity). (A) Representative images showing type I collagen deposition (by immunofluorescence) in these cells after osteogenic induction and bar graphs showing the result of the quantitative analysis (Bars: 200 μm). A negative immunocytochemical control (-Control) is shown. Data are mean±SEM (n = 9). $P < 0.01$: *vs.* cells cultured in the absence of BAPN. Significant differences were determined using unpaired t test. (B) Representative images showing extracellular matrix (ECM) mineralization (by Alizarin Red (A.R.) staining) after osteogenic induction, and bar graphs showing the result of the quantitative analysis. Data are mean±SEM (n = 9). $P < 0.01$: *vs.* cells cultured in the absence of BAPN. Significant differences were determined using Mann-Whitney test. (C) Representative images showing AR staining of VICs cultured on ECM from VICs cultured in the presence (ECM-BAPN) or absence of BAPN (ECM) and exposed to osteogenic medium. Data are mean±SEM (n = 10). $P < 0.01$: *vs.* cells cultured on ECM from VICs non-exposed to BAPN. Bars: 100 μm. Significant differences were determined using unpaired t test.

(Supplementary Fig. S7A), and grossly visible once the mice were sacrificed, in either the aortic arch and its branches (Supplementary Fig. S7B). Importantly, the quantitative analysis of atherosclerosis burden by en face ORO staining of the whole aorta revealed that LOX transgenesis increases atherosclerosis mainly in the abdominal aorta (Fig. 7A-B). In fact, analysis in longitudinal sections of the aortic arch revealed no differences in atherosclerotic lesion area between WT and LOX transgenic mice. However, $TgLOX^{VSMC}$ animals exhibited higher macrophage infiltration and enhanced content of α-SMA positive cells than WT ones (Fig. 7C). Comparable results were obtained in brachiocephalic arteries in which LOX transgenesis did not influence lesion size, but increased macrophage content, total α-SMA positive cell area, and fibrous cap thickness (Supplementary Fig. S8).

We assessed the impact of LOX on vascular calcification in atherosclerosis-challenged $TgLOX^{VSMC}$ mice. $PCSK9^{D374Y}$ transduction combined with a HF/HC diet in mice did not affect plasma calcium levels, but similarly disturbed other specific circulating parameters related to calcium metabolism in both WT and LOX transgenic mice, decreasing DKK-1 plasma levels and increasing those of phosphate and OPG (Supplementary Fig. S9). Vascular osteogenic activity was determined using the fluorescent calcium tracer Osteosense™ 680EX that binds hydroxyapatite crystals and provides a specific and sensible tool to quantify vessel calcification [42]. Osteosense™ 680EX was administered 24 h before the end of the experimental approach and, subsequently, dissected aortas were imaged. As shown in Fig. 8A, NIRF analysis evidenced higher calcium deposition throughout the entire aorta and, in particular, in the aortic arch from LOX transgenic mice. Consistently, plaque calcium deposition assessed by either von Kossa or Osteosense™ 680EX stainings was more prominent in aortic arch sections from $TgLOX^{VSMC}$ mice than in those from control animals (Fig. 8B), associated with higher RUNX2 expression (Fig. 8C). More extensive aortic calcifications were also apparent in brachiocephalic

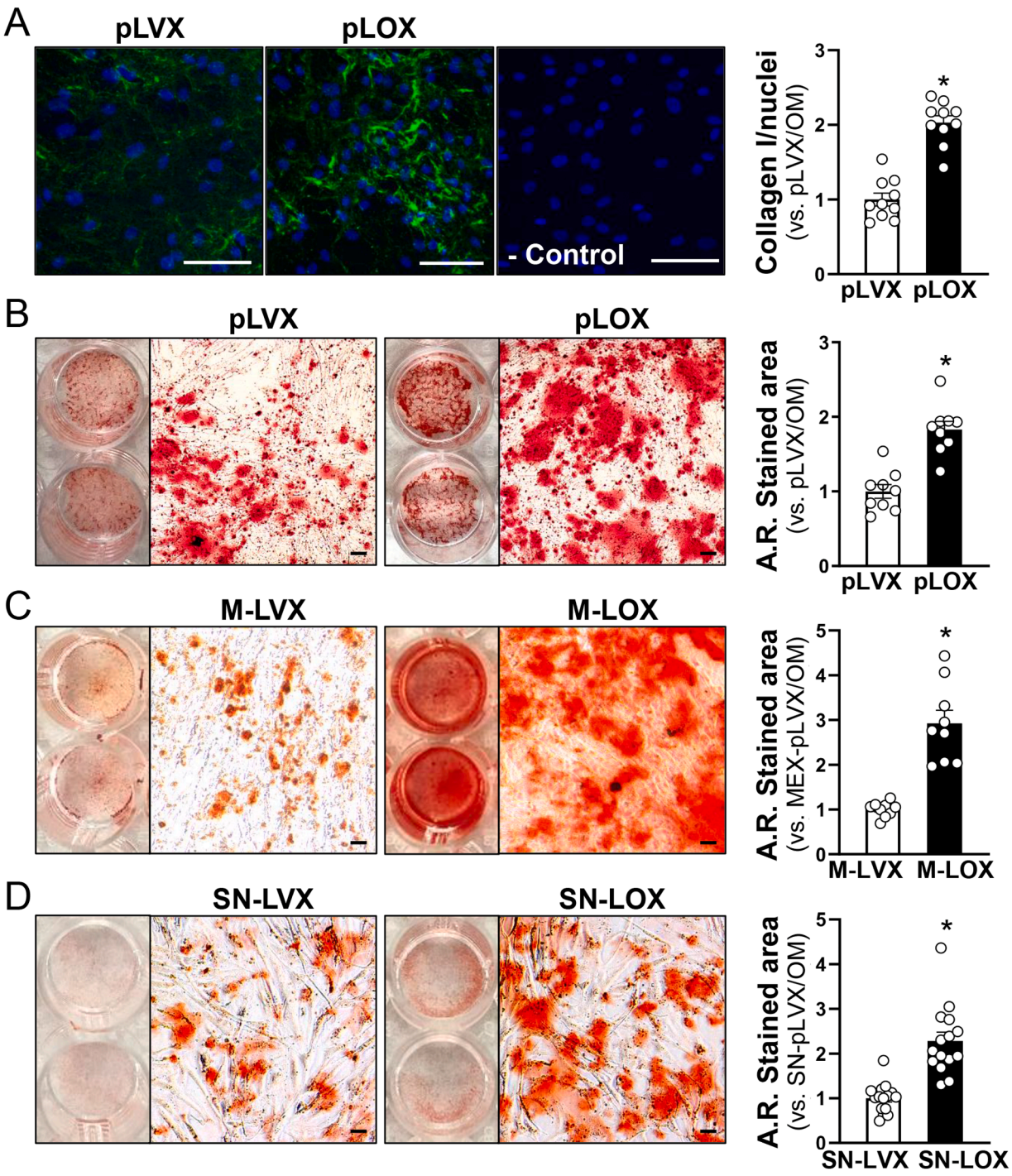

Fig. 5. LOX overexpression enhances valvular interstitial cells (VICs) calcification. (A-B) Human VICs were transduced with pLVX (empty vector) or pLVX-LOX (pLOX) lentivirus and were cultured under osteogenic conditions. (A) Representative images showing type I collagen deposition (by immunofluorescence; n = 10) after osteogenic induction, and bar graphs showing the result of the quantitative analysis. A negative immunocytochemical control (- Control) is shown (Bars: 200 μm). Data are mean±SEM. $P < 0.0001$: *vs. cells transduced with pLVX and exposed to osteogenic medium. Significant differences were determined using unpaired t test. (B) Representative images showing extracellular matrix (ECM) mineralization (by Alizarin Red (AR) staining; lower panels; n = 9) after osteogenic induction, and bar graphs showing the result of the quantitative analysis. Data are mean±SEM. $P < 0.0001$: *vs. cells transduced with pLVX and exposed to osteogenic medium. Significant differences were determined using unpaired t test. (C) Representative images showing AR staining of VICs cultured on ECM from VICs transduced with pLVX (M-LVX) or pLOX lentivirus (M-LOX) and exposed to osteogenic medium. Data are mean±SEM (n = 9). $P < 0.0001$: *vs. cells cultured on M-LVX and exposed to osteogenic medium. Significant differences were determined using unpaired t-test. (D) Representative images showing AR staining of VICs exposed to osteogenic medium supplemented with cell supernatants from VICs transduced with pLVX (SN-LVX) or pLOX lentivirus (SN-LOX). Data are mean±SEM (n = 15). $P < 0.0001$: *vs. cells exposed to osteogenic medium supplemented with SN-LVX. Bars: 100 μm. Significant differences were determined by Mann-Whitney test.

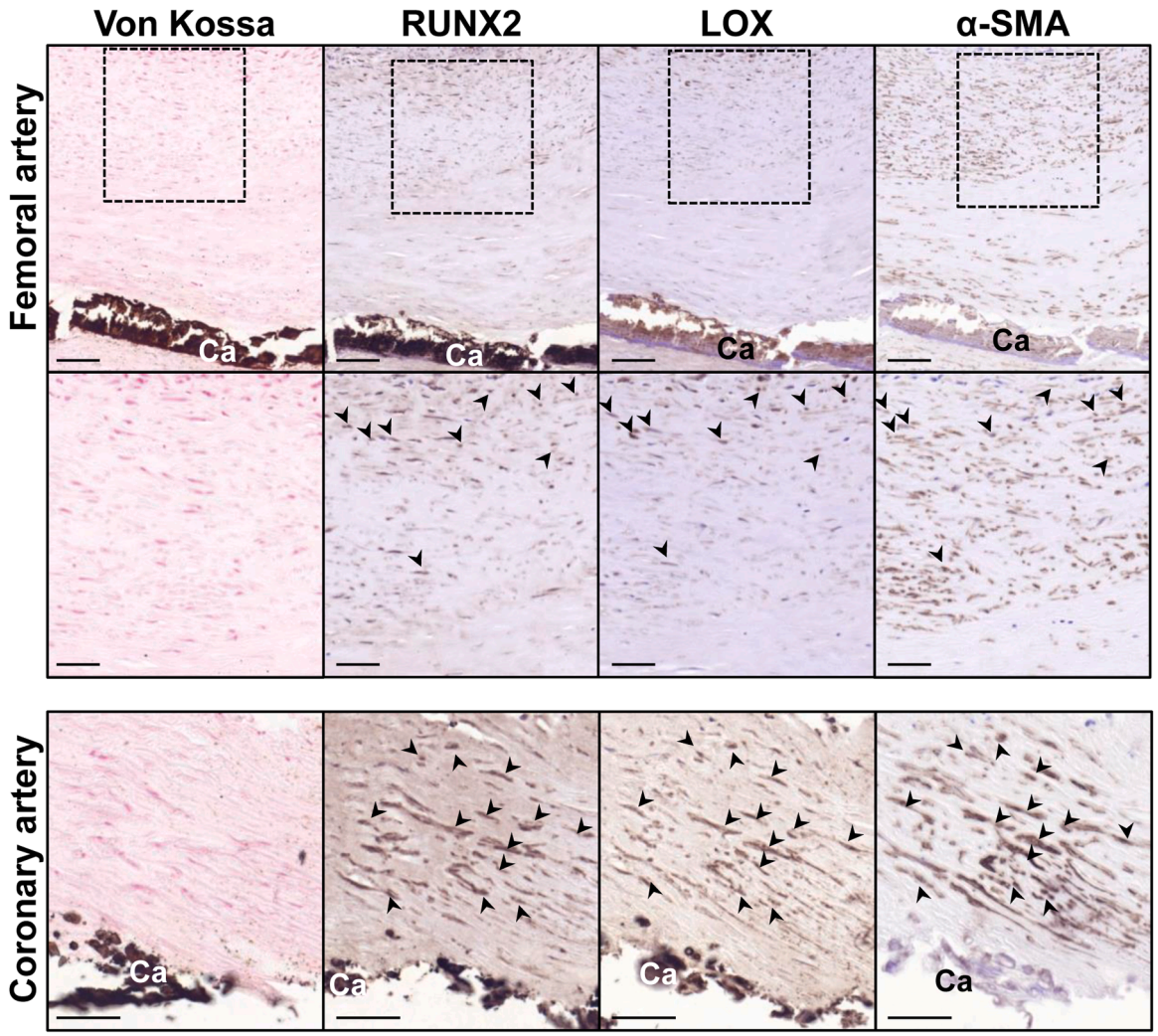

Fig. 6. LOX and RUNX2 are upregulated in calcified human arteries. Representative images of Von Kossa staining and immunostainings for RUNX2, LOX and α-smooth muscle actin (α-SMA) in calcified human arteries. The indicated areas are magnified in middle panels. Black arrowheads indicate positive cells for RUNX2, LOX and α-SMA detected in consecutive sections. Bars: 100 μm (upper panels) and 50 μm (central and lower panels).

atheromatous lesions from LOX transgenic mice which also exhibited enhanced expression of RUNX2 (Fig. 9). It should be noted, that LOX transgenesis is accompanied by a significant increase in mature collagen content in atherosclerotic plaques from both the aortic arch and brachiocephalic trunk associated with a more extensive alcian blue stained area, indicative of higher amounts of mucoid material (Figs. 8 and 9). This increase in crosslinked collagen was also detected in atheromatous lesions from the aortic root accompanied by higher ROS production (Supplementary Fig. S10), although no aortic root calcification was detected under our experimental conditions.

4. Discussion

ECM is an active player in CVC, a major public health issue with an unmet need for effective therapies. The EMC-modifying enzyme LOX is involved in the pathophysiological mechanisms underlying cardiovascular diseases, and recently we have described that LOX-mediated collagen crosslinking would be a critical factor in VSMC calcification [18,20]. However, the contribution of LOX to intimal calcification within atherosclerotic plaques is unknown and its role in CAVD is virtually unexplored. In this study, we show that LOX is strikingly expressed in human calcified aortic valves and atherosclerotic arteries and, complementary *in vitro* and in *vivo* approaches, uncover the role of LOX-dependent ECM crosslinking controlling calcification in atherosclerosis and aortic valve disease.

LOX activity is a critical determinant of pathological collagen crosslinking and fibrosis in different disorders [20,23]; however, few studies have addressed the contribution of this enzyme to the fibrocalcific remodeling of CAVD. Previous research reported no differences in LOX expression between healthy and diseased valves [43]. Here, analysis in valve leaflets from two independent cohorts of CAVD patients allowed us to characterize the relative expression pattern of LOX family members. LOX was the main isoenzyme in healthy valves and was the most overexpressed isoform in highly calcified samples. Close to the calcified area of these valves, LOX localizes to VICs positive for RUNX2, the master transcription factor orchestrating CAVD [12], thus suggesting the contribution of LOX to this disorder. In fact, calcifying human VICs secrete large amounts of LOX, while gain- and loss-of function studies in these cells confirmed the active involvement of LOX in matrix mineralization. Pharmacological inhibition of LOX was achieved using BAPN, an irreversible inhibitor of LOX activity [20], that has been extensively used to support the role of LOXs in different diseases [30,36,43,44]. BAPN inhibited VICs' mineralization, and considering the striking induction of LOX in these cells, the huge effect of BAPN on calcium deposition supports a prominent role of this isoenzyme in the process. This was subsequently confirmed by lentiviral transduction showing that LOX overexpression aggravated OM-induced matrix mineralization.

Of note, immunofluorescence analysis in nonpermeabilized

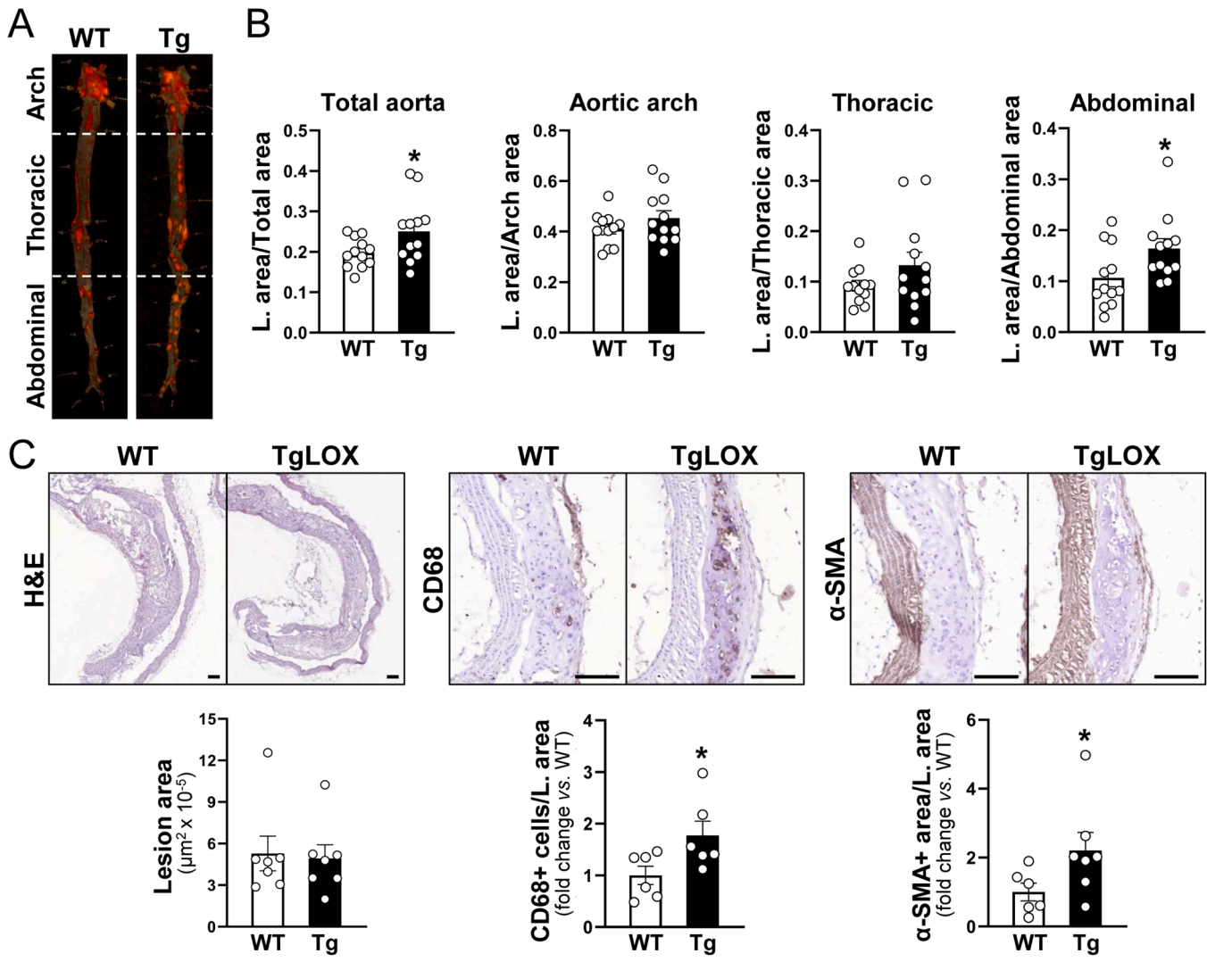

Fig. 7. LOX transgenesis enhances atherosclerosis. Wild-type (WT) and TgLOX^{VSMC} (Tg) mice were subjected to a single tail vein injection of adeno-associated viruses (AAV) encoding for PCSK9^{D374Y} (AAV-PCSK9^{D374Y}) combined with a high fat/high cholesterol (HF/HC) diet for 20 weeks. (A) Representative images of en face Oil Red O (ORO) aorta stainings (dotted lines indicating the areas corresponding to aortic arch, thoracic aorta and abdominal aorta), and (B) bar graphs showing the results of the quantitative analysis for the whole aorta and these areas. Results are mean±SEM (n = 12). * $P < 0.05$ *vs.* PCSK9^{D374Y}-transduced WT mice. (C) Representative images of hematoxylin & eosin and immunohistochemical staining of aortic arch sections from these animals used to determine lesion area and to estimate the content of macrophages (CD68) and vascular smooth muscle cells (alpha-smooth muscle actin [α-SMA] positive cells), and bar graphs showing the result of the quantitative analyses (at least n = 6). Results are mean±SEM. * $P < 0.05$ *vs.* PCSK9^{D374Y}-transduced WT mice. Bars: 100 μm. Significant differences were determined by Mann-Whitney test (B and C) or unpaired t-test (Total aorta in B).

calcifying VICs revealed that LOX inhibition/overexpression was associated with consistent changes in the organization and quantity of layered collagen. Beyond its role in ECM maturation, in the last years additional intracellular functions have been attributed to LOX [20–23, 45]. In this regard, our studies in cell-denuded matrices evidenced that the LOX-mediated remodeling of the ECM guides VICs' mineralization and this would explain the great impact on calcification observed in both BAPN-treated and LOX-overexpressing cells. Given that LOX activity is closely related to matrix stiffening [30,31,44,46,47], these results are in accordance with the spontaneous calcification observed in porcine VICs cultured on stiff surfaces [48]. Further and because conditioned media from LOX-transduced VICs intensified matrix calcification, our data strengthen the concept that the pro-calcifying activity of LOX relies on the extracellular and active form of this enzyme. Therefore, our results support that extracellular LOX impacts on matrix remodeling and that this mechanism would drive VICs' calcification.

LOX is downregulated by atherosclerotic risk factors and it has been suggested that altered LOX activity could be linked to virtually all stages of the atherosclerotic process [20–23]. However, data from human studies or animal models regarding the specific impact of LOX on atherosclerosis and its relevance to VC are scarce. In human carotid endarterectomy specimens, the expression of LOX in areas with ongoing fibrogenesis suggested that LOX-mediated collagen cross-linking might favor the healing of human atherosclerotic lesions [49]. Moreover, we reported high expression of LOX in calcified atheromas from femoral and popliteal arteries that positively correlated with the degree of vascular calcification [18]. Here, we confirm these insights and extend our findings to human coronary arteries. In both calcified femoral and coronary atherosclerotic plaques, LOX was highly expressed and colocalized with VSMCs positive for RUNX2, a transcription factor essential for the osteogenic transdifferentiation and calcification not only of VICs (in aortic valves) but also of VSMCs (in atherosclerotic lesions) [11]. No studies, however, have addressed whether LOX impacts on atherosclerosis and intimal calcification in preclinical models. Early studies from Kothapalli and col. reported that LOX upregulation underlies arterial stiffness in apolipoprotein E (ApoE) null mice and that its

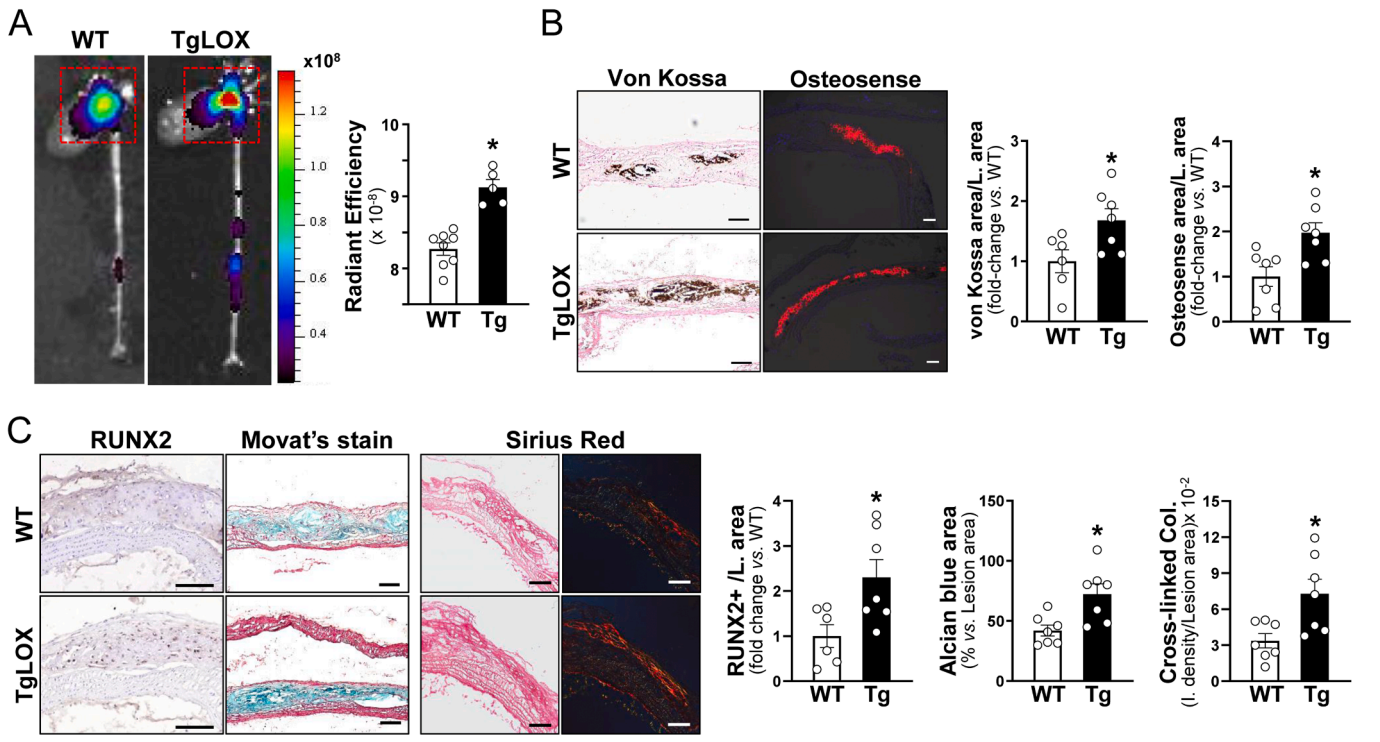

Fig. 8. LOX transgenesis enhances vascular calcification. WT and TgLOX^{VSMC} (Tg) mice were subjected to a single tail vein injection of adeno-associated viruses (AAV) encoding for PCSK9^{D374Y} (AAV-PCSK9^{D374Y}) combined with a high fat/high cholesterol (HF/HC) diet for 20 weeks. (A) Representative images of the *ex vivo* near-infrared fluorescence reflectance imaging (NIRF) analysis of aortas from WT and TgLOX^{VSMC} mice transduced with AAV-PCSK9^{D374Y} and injected with the fluorescence calcium tracer OsteoSense™ 680EX 24 h before the end of the experimental protocol. Bar graph on the right shows the result of the quantification of NIRF images. Results are mean±SEM (WT n = 8; Tg n = 5). * $P < 0.01$ *vs*. WT mice. (B) Representative images of von Kossa and OsteoSense™ 680EX stainings used to determine vascular calcification in aortic arch sections WT and TgLOX^{VSMC} mice transduced with AAV-PCSK9^{D374Y}. Bar graphs on the right show the result of the quantitative analysis. (C) Representative images of RUNX2 immunostainings and Movat's and Sirius Red stainings of aortic arch sections from these animals. Sirius Red staining was captured under both bright field (left panel) and polarized light to estimate collagen cross-linking (Cross-linked col.) (right panel). Bar graphs on the bottom show the result of the quantitative analyses. Data are mean±SEM. * $P < 0.05$ *vs*. WT mice (at least n = 6). Bars: 100 μm. Significant differences were determined by the Mann-Whitney test (A to C).

pharmacological inhibition attenuates vascular stiffness and atherosclerosis [30]. However, ApoE itself inhibits the expression of LOX [30] which disqualifies the ApoE knockout mouse as a model to rigorously analyze the contribution of LOX to atherosclerosis. Therefore, we explored this issue by inducing atherosclerosis in our transgenic mouse model that overexpresses LOX in VSMC (TgLOX^{VSMC}). For this purpose, we induced hypercholesterolemia and atherosclerosis in C57BL/6 J mice using an approach that circumvents the need of cross-breeding with an atherosclerosis prone strain (*e.g.*, ApoE$^{-/-}$).[27,28] This strategy, which involves the administration of a single injection of a gain-of-function mutant of human PCSK9 protein (AAV-PCSK9^{D374Y}) combined with a HF/HC diet, has been previously validated to assess atherosclerosis and calcification [37,38,41]. This approach strikingly reduced hepatic LDLR levels and raised plasma lipids, reaching in few days a similar steady-state level in both WT and transgenic animals, and at the end of the study, producing a comparable impact on mineral metabolism biomarkers in both groups. Nevertheless, LOX transgenesis slightly increased atherosclerosis and strongly exacerbated intimal calcification, leading to more inflamed lesions with more cross-linked ECM and thicker fibrous caps. Indeed, using Osteosense 680 EX, a probe that specifically binds to hydroxyapatite crystals improving sensitivity and quantitative assessment of tissue mineralization [42,50], we showed that LOX transgenesis enhanced calcification assessed by *ex vivo* NIRF reflectance imaging of the whole aorta, and by fluorescence microscopy in aortic arch longitudinal sections. Of note, Von Kossa staining, a classical method extensively used to detect ectopic calcification in soft tissues, also noticed increased calcification in vascular sections from TgLOX^{VSMC} mice. Recently, a study in rats using a warfarin-induced calcification-model revealed that BAPN attenuated aortic medial calcification [51]. Therefore, LOX seems to play a critical role in both intimal and medial calcification. Finally, in both CAVD and atherosclerotic lesions, areas highly positive for LOX also exhibited high ROS production, which is in agreement with results reported in other pathological scenarios [33,34,52], and is coherent with the fact that LOX activity is a source of oxidative stress [30].

Early studies by Aikawa and coworkers supported the link between vascular inflammation and calcification [53]. This relationship in animal models, subsequently confirmed in patients [54], suggests that inflammation precedes and drives calcification. Consistent with this, atherosclerotic lesions from TgLOX^{VSMC} mice were more inflamed that those from WT mice, although our data did not allow to establish a temporal relationship between inflammation and calcification. It should be noted that LOX is a potent chemoattractant for human monocytes and VSMCs [55,56], which could explain the increased macrophage infiltration and both the higher thickening of the fibrous cap and the greater VSMC content of atherosclerotic plaques from TgLOX^{VSMC} mice, even though we and others have reported an anti-proliferative effect of LOX on VSMC cultures [28,29,57]. Finally, the present study showed that atheromatous lesions from transgenic mice exhibited a higher degree of collagen crosslinking and higher glycosaminoglycan content than lesions from WT animals. In agreement, our previous studies have shown that VSMC calcification involves increased deposition of organized collagen that requires upregulation of lysyl hydroxylase 1 and LOX [18], key enzymes for the post-translational processing of collagen, a process that is essential in the biogenesis of a mature ECM. In fact, VSMC isolated from TgLOX^{VSMC} mice exhibited higher collagen deposition,

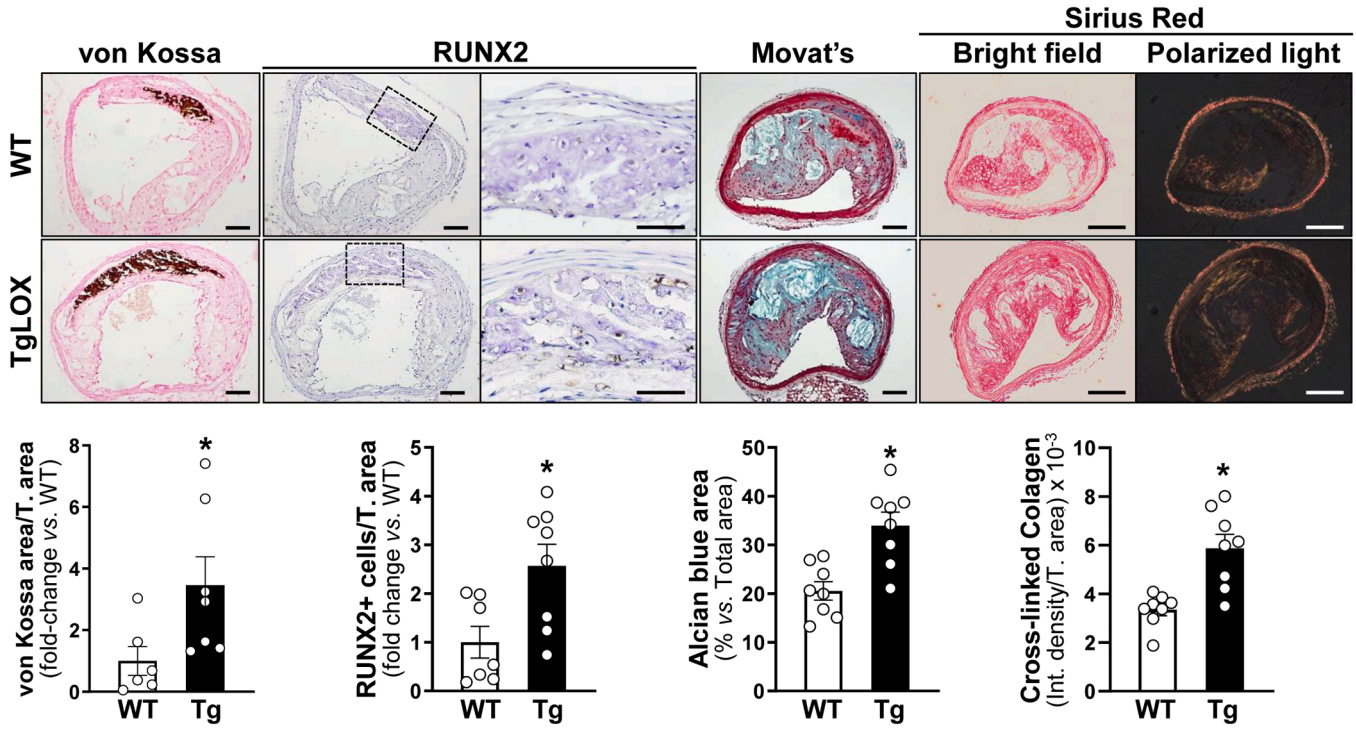

Fig. 9. Impact of LOX transgenesis on vascular calcification in the brachiocephalic artery. WT and TgLOX^{VSMC} (Tg) mice were subjected to a single tail vein injection of an adeno-associated virus (AAV) vector encoding for PCSK9^{D374Y} (AAV-PCSK9^{D374Y}) combined with a high fat/high cholesterol (HF/HC) diet for 20 weeks and the brachiocephalic artery was dissected. Calcification was assessed by von Kossa staining. RUNX2 positive cells (the indicated area is shown magnified on the right panels, bars: 50 μm), and both Movat's and Sirius Red stainings are shown. Sirius Red staining was visualized under both bright field and polarized light. Bars: 100 μm. Histograms show the quantitative analysis. Results are mean±SEM. *P < 0.05 *vs.* PCSK9^{D374Y}-transduced WT mice (at least n = 6). Significant differences were determined by the Mann-Whitney test.

enhanced ECM mineralization and increased expression of osteogenic markers than WT cells, responses that were prevented when LOX activity was pharmacologically inhibited [18]. Our present studies in LOX transgenic mice further underscore the importance of ECM in VC and emphasize the interest of LOX as a potential therapeutic target in intimal calcification associated with atherosclerosis.

In summary, huge progress has been made over the last years in unraveling the mechanisms involved in CVC. The present study provides *in vitro* and *in vivo* evidence about the critical role of LOX in both CAVD and CV, highlights LOX-dependent ECM remodeling as a key step for matrix mineralization in these pathologies and suggest the potential involvement of other mechanisms influenced by LOX such as vascular inflammation and oxidative stress. Further research is guaranteed to characterize in depth the molecular mechanisms underlying the impact of LOX on CVC, but the present study suggests that CVC might be controlled by locally modulating the organization of the ECM that originates the foci of calcification.

CRediT authorship contribution statement

C.R. and J.M.-G. conceived the study, designed the experiments, acquired the financial support and wrote the manuscript. C.B.-S, J.A., L. P.-U, A.R.-S. and L.C., performed the *in vivo* studies and acquired data. C. B.-S, P.V.-S. and L.C. carried out cell culture studies. M.T., N.L.-A. and A. F.-C. participated in patient recruitment, sample processing and supervised the clinical aspects of the research. C.B.-S, L.C. and A.F.-C. analyzed human samples. All the authors read and approved the final manuscript.

Declaration of Competing Interest

The authors declare that they have no conflict of interest.

Data Availability

Data will be made available on request.

Acknowledgments

We thank the technical support provided by Silvia Aguiló. This work was supported by the Spanish Ministerio de Ciencia e Innovación (RTI2018-094727-B-100 and PID2021-122509OB-I00 funded by MCIN/AEI/10.13039/501100011033 and by "ERDF A way of making Europe"), Instituto de Salud Carlos III (ISCIII; Spain; PI21/01048), and Fundación Española de Arteriosclerosis (FEA-2022). C.B-S and L.P-U were supported by a FPU (Ministerio de Universidades; Spain), and PFIS (ISCIII) fellowships, respectively and N.L-A by a Miguel Servet contract (ISCIII). There is no financial or personal relationship with organizations that could potentially influence the described research.

Appendix A. Supporting information

Supplementary data associated with this article can be found in the online version at doi:10.1016/j.biopha.2023.115469.

References

[1] A. Kelly-Arnold, N. Maldonado, D. Laudier, E. Aikawa, L. Cardoso, S. Weinbaum, Revised microcalcification hypothesis for fibrous cap rupture in human coronary arteries, Proc. Natl. Acad. Sci. USA 110 (26) (2013) 10741–10746.
[2] A. Corti, A. De Paolis, P. Grossman, P.A. Dinh, E. Aikawa, S. Weinbaum, L. Cardoso, The effect of plaque morphology, material composition and microcalcifications on the risk of cap rupture: A structural analysis of vulnerable atherosclerotic plaques, Front. Cardiovasc. Med. 9 (2022) 1019917.
[3] C. Shekar, M. Budoff, Calcification of the heart: mechanisms and therapeutic avenues, Expert. Rev. Cardiovasc. Ther. 16 (7) (2018) 527–536.
[4] P. Greenland, M.J. Blaha, M.J. Budoff, R. Erbel, K.E. Watson, Coronary calcium score and cardiovascular risk, J. Am. Coll. Cardiol. 72 (2018) 434–447.

[5] B.R. Lindman, D. Sukul, M.R. Dweck, M.V. Madhavan, B.J. Arsenault, M. Coylewright, W.D. Merryman, D.E. Newby, J. Lewis, F.E. Harrell Jr., M.J. Mack, M.B. Leon, C.M. Otto, P. Pibarot, Evaluating medical therapy for calcific aortic stenosis: JACC state-of-the-art review, J. Am. Coll. Cardiol. 78 (23) (2021) 2354–2376.
[6] S. Shu, Y. Yang, B. Sun, Z. Su, M. Fu, C. Xiong, X. Zhang, S. Hu, J. Song J, Alerting trends in epidemiology for calcific aortic valve disease, 1990-2019: an age-period-cohort analysis for the Global Burden of Disease Study 2019, Eur. Heart J. Qual. Care Clin. Outcomes 9 (2023) 459–473.
[7] M.A. Rogers, E. Aikawa, Cardiovascular calcification: artificial intelligence and big data accelerate mechanistic discovery, Nat. Rev. Cardiol. 16 (2019) 261–274.
[8] P.R. Goody, M.R. Hosen, D. Christmann, S.T. Niepmann, A. Zietzer, M. Adam, F. Bönner, S. Zimmer, G. Nickenig, F. Jansen, Aortic valve stenosis: from basic mechanisms to novel therapeutic targets, Arterioscler. Thromb. Vasc. Biol. 40 (2020) 885–900.
[9] L.M. Moncla, M. Briend, Y. Bossé, P. Mathieu, Calcific aortic valve disease: mechanisms, prevention and treatment, Nat. Rev. Cardiol. 20 (8) (2023) 546–559.
[10] F. Buffolo, S. Monticone, G. Camussi, E. Aikawa, Role of extracellular vesicles in the pathogenesis of vascular damage, Hypertension 79 (5) (2022) 863–873.
[11] Y. Chen, X. Zhao, H. Wu, Transcriptional programming in arteriosclerotic disease: a multifaceted function of the Runx2 (Runt-related transcription factor 2), Arterioscler. Thromb. Vasc. Biol. 41 (2021) 20–34.
[12] S. Dharmarajan, M.Y. Speer, K. Pierce, J. Lally, E.M. Leaf, M.E. Lin, M. Scatena, C. M. Giachelli, Role of Runx2 in calcific aortic valve disease in mouse models, Front. Cardiovasc. Med. 8 (2021), 687210.
[13] Y. Qian, L. Li, Z. Sun, J. Liu, W. Yuan, Z. Wang, A multi-omics view of the complex mechanism of vascular calcification, Biomed. Pharmacother. 135 (2021), 111192.
[14] J. Zhang, Y. Ji, S. Jiang, M. Shi, W. Cai, R.J. Miron, Y. Zhang, Calcium–collagen coupling is vital for biomineralization schedule, Adv. Sci. 8 (15) (2021), e2100363.
[15] K.H. Müller, R. Hayward, R. Rajan, M. Whitehead, A.M. Cobb, S. Ahmad, M. Sun, I. Goldberga, R. Li, U. Bashtanova, A.M. Puszkarska, D.G. Reid, R.A. Brooks, J. N. Skepper, J. Bordoloi, W.Y. Chow, H. Oschkinat, A. Groombridge, O. A. Scherman, J.A. Harrison, A. Verhulst, P.C. D'Haese, E. Neven, L.M. Needham, S. F. Lee, C.M. Shanahan, M.J. Duer, Poly(ADP-Ribose) Links the DNA damage response and biomineralization, Cell Rep. 27 (11) (2019) 3124–3138.e13.
[16] M.E. Schroeder, A. Gonzalez Rodriguez, K.F. Speckl, C.J. Walker, F.S. Midekssa, J. C. Grim, R.M. Weiss, K.S. Anseth, Collagen networks within 3D PEG hydrogels support valvular interstitial cell matrix mineralization, Acta Biomater. 119 (2021) 197–210.
[17] A. Di Vito, A. Donato, I. Presta, T. Mancuso, F.S. Brunetti, P. Mastroroberto, A. Amorosi, N. Malara, G. Donato, Extracellular matrix in calcific aortic valve disease: architecture, dynamic and perspectives, Int. J. Mol. Sci. 22 (2) (2021) 913.
[18] E. Jover, A. Silvente, F. Marín, J. Martínez-González, M. Orriols, C.M. Martinez, C. M. Puche, M. Valdés, C. Rodriguez, D. Hernández-Romero D, Inhibition of enzymes involved in collagen cross-linking reduces vascular smooth muscle cell calcification, FASEB J. 32 (8) (2018) 4459–4469.
[19] Y. Xue, A.P. Kossar, A. Abramov, A. Frasca, M. Sun, M. Zyablitskaya, D. Paik, D. Kalfa, M. Della Barbera, G. Thiene, S. Kozaki, T. Kawashima, J.H. Gorman, R. C. Gorman, M.J. Gillespie, C.K. Carreon, S.P. Sanders, R.J. Levy, G. Ferrari, Age-related enhanced degeneration of bioprosthetic valves due to leaflet calcification, tissue crosslinking, and structural changes, Cardiovasc. Res. 119 (1) (2023) 302–315.
[20] C. Rodríguez, A. Rodríguez-Sinovas, J. Martínez-González, Lysyl oxidase as a potential therapeutic target, Drug N. Perspect. 21 (4) (2008) 218–224.
[21] C. Rodríguez, J. Martínez-González, B. Raposo, J.F. Alcudia, A. Guadall, L. Badimon, Regulation of lysyl oxidase in vascular cells: lysyl oxidase as a new player in cardiovascular diseases, Cardiovasc. Res. 79 (1) (2008) 7–13.
[22] J. Martínez-González, S. Varona, L. Cañes, M. Galán, A.M. Briones, V. Cachofeiro, C. Rodríguez, Emerging roles of lysyl oxidases in the cardiovascular system: new concepts and therapeutic challenges, Biomolecules 9 (10) (2019) 610.
[23] C. Rodríguez, J. Martínez-González, The role of lysyl oxidase enzymes in cardiac function and remodeling, Cells 8 (12) (2019) 1483.
[24] C. Rodríguez, B. Raposo, J. Martínez-González, L. Casaní, L. Badimon, Low density lipoproteins downregulate lysyl oxidase in vascular endothelial cells and the arterial wall, Arterioscler. Thromb. Vasc. Biol. 22 (9) (2002) 1409–1414.
[25] B. Raposo, C. Rodríguez, J. Martínez-González, L. Badimon, High levels of homocysteine inhibit lysyl oxidase (LOX) and downregulate LOX expression in vascular endothelial cells, Atherosclerosis 177 (1) (2004) 1–8.
[26] C. Rodríguez, J.F. Alcudia, J. Martínez-González, A. Guadall, B. Raposo, S. Sánchez-Gómez, L. Badimon, Statins normalize vascular lysyl oxidase down-regulation induced by proatherogenic risk factors, Cardiovasc. Res. 83 (3) (2009) 595–603.
[27] C. Rodríguez, J.F. Alcudia, J. Martínez-González, B. Raposo, M.A. Navarro, L. Badimon, Lysyl oxidase (LOX) down-regulation by TNFalpha: a new mechanism underlying TNFalpha-induced endothelial dysfunction, Atherosclerosis 196 (2) (2008) 558–564.
[28] M. Orriols, A. Guadall, M. Galán, I. Martí-Pàmies, S. Varona, R. Rodríguez-Calvo, A.M. Briones, M.A. Navarro, A. de Diego, J. Osada, J. Martínez-González, C. Rodríguez, Lysyl oxidase (LOX) in vascular remodelling. Insight from a new animal model, Thromb. Haemost. 112 (4) (2014) 812–824.
[29] S. Varona, M. Orriols, M. Galán, A. Guadall, L. Cañes, S. Aguiló, M. Sirvent, J. Martínez-González, C. Rodríguez, Lysyl oxidase (LOX) limits VSMC proliferation and neointimal thickening through its extracellular enzymatic activity, Sci. Rep. 8 (1) (2018), 13258.
[30] S. Martínez-Revelles, A.B. García-Redondo, M.S. Avendaño, S. Varona, T. Palao, M. Orriols, F.R. Roque, A. Fortuño, R.M. Touyz, J. Martínez-González, M. Salaices, C. Rodríguez, A.M. Briones, Lysyl oxidase induces vascular oxidative stress and contributes to arterial stiffness and abnormal elastin structure in hypertension: role of p38MAPK, Antioxid. Redox Signal. 27 (7) (2017) 379–397.
[31] S. Chandrakumar, I.S. Tierno, M. Agarwal, N. Matisioudis, T.S. Kern, K. Ghosh, Subendothelial matrix stiffening by lysyl oxidase enhances RAGE-mediated retinal endothelial activation in diabetes, Diabetes 72 (7) (2023) 973–985.
[32] R.K. Sharma, S.H. Kamble, S. Krishnan, J. Gomes, B. To, S. Li, I.C. Liu, M.L. Gumz, R. Mohandas, Involvement of lysyl oxidase in the pathogenesis of arterial stiffness in chronic kidney disease, Am. J. Physiol. Ren. Physiol. 324 (4) (2023) F364–F373.
[33] M. Galán, S. Varona, A. Guadall, M. Orriols, M. Navas, S. Aguiló, A. de Diego, M. A. Navarro, D. García-Dorado, A. Rodríguez-Sinovas, J. Martínez-González, C. Rodriguez, Lysyl oxidase overexpression accelerates cardiac remodeling and aggravates angiotensin II-induced hypertrophy, FASEB J. 31 (9) (2017) 3787–3799.
[34] E. Martínez-Martínez, C. Rodríguez, M. Galán, M. Miana, R. Jurado-López, M. V. Bartolomé, M. Luaces, F. Islas, J. Martínez-González, N. López-Andrés, V. Cachofeiro, The lysyl oxidase inhibitor (β-aminopropionitrile) reduces leptin profibrotic effects and ameliorates cardiovascular remodeling in diet-induced obesity in rats, J. Mol. Cell. Cardiol. 92 (2016) 96–104.
[35] J.R. Sádaba, E. Martínez-Martínez, V. Arrieta, V. Álvarez, A. Fernández-Celis, J. Ibarrola, A. Melero, P. Rossignol, V. Cachofeiro, N. López-Andrés, Role for galectin-3 in calcific aortic valve stenosis, J. Am. Heart Assoc. 5 (11) (2016), e004360.
[36] M. Miana, M. Galán, E. Martínez-Martínez, S. Varona, R. Jurado-López, B. Bausa-Miranda, A. Antequera, M. Luaces, J. Martínez-González, C. Rodríguez, V. Cachofeiro, The lysyl oxidase inhibitor β-aminopropionitrile reduces body weight gain and improves the metabolic profile in diet-induced obesity in rats, Dis. Model. Mech. 8 (6) (2015) 543–551.
[37] M.M. Bjørklund, A.K. Hollensen, M.K. Hagensen, F. Dagnaes-Hansen, C. Christoffersen, J.G. Mikkelsen, J.F. Bentzon, Induction of atherosclerosis in mice and hamsters without germline genetic engineering, Circ. Res. 114 (11) (2014) 1684–1689.
[38] M. Roche-Molina, D. Sanz-Rosa, F.M. Cruz, J. García-Prieto, S. López, R. Abia, F. J. Muriana, V. Fuster, B. Ibáñez, J.A. Bernal, Induction of sustained hypercholesterolemia by single adeno-associated virus-mediated gene transfer of mutant hPCSK9, Arterioscler. Thromb. Vasc. Biol. 35 (1) (2015) 50–59.
[39] M. Garaikoetxea, E. Martín-Núñez, A. Navarro, L. Matilla, A. Fernández-Celis, V. Arrieta, A. García-Peña, A. Gainza, V. Álvarez, R. Sádaba, E. Jover, N. López-Andrés, Targeting fatty acid-binding protein 4 improves pathologic features of aortic stenosis, Int. J. Mol. Sci. 23 (15) (2022) 8439.
[40] N.M. Rajamannan, M. Subramaniam, D. Rickard, S.R. Stock, J. Donovan, M. Springett, T. Orszulak, D.A. Fullerton, A.J. Tajik, R.O. Bonow, T. Spelsberg, Human aortic valve calcification is associated with an osteoblast phenotype, Circulation 107 (17) (2003) 2181–2184.
[41] C. Goettsch, J.D. Hutcheson, S. Hagita, M.A. Rogers, M.D. Creager, T. Pham, J. Choi, A.K. Mlynarchik, B. Pieper, M. Kjolby, M. Aikawa, E. Aikawa, A single injection of gain-of-function mutant PCSK9 adeno-associated virus vector induces cardiovascular calcification in mice with no genetic modification, Atherosclerosis 251 (2016) 109–118.
[42] A. Greco, J. Herrmann, M. Babic, M.R. Gummi, M. van der Giet, M. Tölle, M. Schuchardt, Molecular imaging and quantification of smooth muscle cell and aortic tissue calcification in vitro and ex vivo with a fluorescent hydroxyapatite-specific probe, Biomedicines 10 (9) (2022) 2271.
[43] H.N. Hutson, T. Marohl, M. Anderson, K. Eliceiri, P. Campagnola, K.S. Masters, Calcific aortic valve disease is associated with layer-specific alterations in collagen architecture, PLoS One 11 (9) (2016), e0163858.
[44] D. Kothapalli, S.L. Liu, Y.H. Bae, J. Monslow, T. Xu, E.A. Hawthorne, F.J. Byfield, P. Castagnino, S. Rao, D.J. Rader, E. Puré, M.C. Phillips, S. Lund-Katz, P.A. Janmey, R.K. Assoian, Cardiovascular protection by ApoE and ApoE-HDL linked to suppression of ECM gene expression and arterial stiffening, Cell Rep. 2 (5) (2012) 1259–1271.
[45] K.R. Levental, H. Yu, L. Kass, J.N. Lakins, M. Egeblad, J.T. Erler, S.F. Fong, K. Csiszar, A. Giaccia, W. Weninger, M. Yamauchi, D.L. Gasser, V.M. Weaver, Matrix crosslinking forces tumor progression by enhancing integrin signaling, Cell 139 (5) (2009) 891–906.
[46] P.C. Trackman, Enzymatic and non-enzymatic functions of the lysyl oxidase family in bone, Matrix Biol. 52–54 (2016) 7–18.
[47] J.H. Kim, G. Lee, Y. Won, M. Lee, J.S. Kwak, C.H. Chun, J.S. Chun, Matrix cross-linking-mediated mechanotransduction promotes posttraumatic osteoarthritis, Proc. Natl. Acad. Sci. USA 112 (30) (2015) 9424–9429.
[48] U. Majumdar, S. Manivannan, M. Basu, Y. Ueyama, M.C. Blaser, E. Cameron, M. R. McDermott, J. Lincoln, S.E. Cole, S. Wood, E. Aikawa, B. Lilly, V. Garg, Nitric oxide prevents aortic valve calcification by S-nitrosylation of USP9X to activate NOTCH signaling, Sci. Adv. 7 (6) (2021), eabe3706.
[49] O.A. Ovchinnikova, L. Folkersen, J. Persson, J.H. Lindeman, T. Ueland, P. Aukrust, N. Gavrisheva, E. Shlyakhto, G. Paulsson-Berne, U. Hedin, P.S. Olofsson, G. K. Hansson, The collagen cross-linking enzyme lysyl oxidase is associated with the healing of human atherosclerotic lesions, J. Intern. Med. 276 (5) (2014) 525–536.
[50] A.M. Sim, N.A. Rashdan, L. Cui, A.J. Moss, F. Nudelman, M.R. Dweck, V. E. MacRae, A.N. Hulme, A novel fluorescein-bisphosphonate based diagnostic tool for the detection of hydroxyapatite in both cell and tissue models, Sci. Rep. 8 (1) (2018), 17360.
[51] K. Uto, S. Yoshizawa, C. Aoki, T. Nishikawa, H. Oda, Inhibition of extracellular matrix integrity attenuates the early phase of aortic medial calcification in a rodent model, Atherosclerosis 319 (2021) 10–20.

[52] L. Valls-Lacalle, L. Puertas-Umbert, S. Varona, J. Martínez-González, C. Rodríguez, A. Rodríguez-Sinovas, Human lysyl oxidase over-expression enhances baseline cardiac oxidative stress but does not aggravate ROS generation or infarct size following myocardial ischemia-reperfusion, Antioxidants 11 (1) (2021) 75.
[53] E. Aikawa, M. Nahrendorf, J.L. Figueiredo, F.K. Swirski, T. Shtatland, R.H. Kohler, F.A. Jaffer, M. Aikawa, R. Weissleder, Osteogenesis associates with inflammation in early-stage atherosclerosis evaluated by molecular imaging in vivo, Circulation 116 (24) (2007) 2841–2850.
[54] A. Abdelbaky, E. Corsini, A.L. Figueroa, S. Fontanez, S. Subramanian, M. Ferencik, T.J. Brady, U. Hoffmann, A. Tawakol, Focal arterial inflammation precedes subsequent calcification in the same location: a longitudinal FDG-PET/CT study, Circ. Cardiovasc. Imaging 6 (5) (2013) 747–754.
[55] H.M. Lazarus, W.W. Cruikshank, N. Narasimhan, H.M. Kagan, D.M. Center, Induction of human monocyte motility by lysyl oxidase, Matrix Biol. 14 (9) (1995) 727–731.
[56] H.A. Lucero, K. Ravid, J.L. Grimsby, C.B. Rich, S.J. DiCamillo, J.M. Mäki, J. Myllyharju, H.M. Kagan, Lysyl oxidase oxidizes cell membrane proteins and enhances the chemotactic response of vascular smooth muscle cells, J. Biol. Chem. 283 (35) (2008) 24103–24117.
[57] Y.X. Qi, J. Jiang, X.H. Jiang, X.D. Wang, S.Y. Ji, Y. Han, D.K. Long, B.R. Shen, Z. Q. Yan, S. Chien, Z.L. Jiang, PDGF-BB and TGF-{beta}1 on cross-talk between endothelial and smooth muscle cells in vascular remodeling induced by low shear stress, Proc. Natl. Acad. Sci. USA 108 (5) (2011) 1908–1913.